Computational Prediction of Water Sorption in Facilitated Transport Membranes

Xuepeng Deng†, Yang Han†, Li-Chiang Lin*†‡, W.S. Winston Ho*†§*

† William G. Lowrie Department of Chemical and Biomolecular Engineering, The Ohio State University, Columbus, Ohio 43210, United States

‡ Department of Chemical Engineering, National Taiwan University, Taipei 10617, Taiwan

§ Department of Materials Science and Engineering, The Ohio State University, Columbus, Ohio 43210, United States

*Corresponding authors: Yang Han (han.779@osu.edu); Li-Chiang Lin (lclin@ntu.edu.tw); W.S. Winston Ho (ho.192@osu.edu).

KEYWORDS: Water sorption; Facilitated transport membrane; Continuous fractional component Monte Carlo; Molecular simulations.

ABSTRACT:

Polymeric facilitated transport membranes (FTMs) have emerged as an innovative class of promising carbon capture technology. Studies have shown that the transport properties of an FTM are significantly influenced by its water uptake. In order to better quantify FTM performance, we herein explore the potential of computational techniques to predict the equilibrium water uptake values of FTMs. Two prediction approaches were examined. First, the water sorption was explicitly simulated by iteratively conducting grand canonical Monte Carlo (GCMC) and molecular dynamics (MD) simulations. Second, the water sorption was predicted based on the chemical potential of the adsorbed water, which was calculated using the Widom insertion or continuous fractional component Monte Carlo (CFCMC) method. The chemical potential-based approach with CFCMC demonstrated good prediction of the equilibrium water uptake values of FTMs with poly(*N*-vinylformamide-*co*-vinylamine) as fixed-site carrier and 2-(1-piperazinyl)ethylamine sarcosinate as mobile carrier. The predicted water uptake values increased with increasing mobile carrier content and were in good agreement with the experimental values. The higher water uptake promoted the diffusion of CO_2, N_2, and mobile carrier as well as slightly stifled the sorption of N_2. Such an approach significantly contributes to a more comprehensive theoretical evaluation of FTMs.

INTRODUCTION

Polymeric facilitated transport membranes (FTMs) are a class of innovative materials that are easy to fabricate[1] and scalable[2], and have shown great promise in separating CO_2 from flue gas[2–7]. Bestowed by the reversible amine–CO_2 chemistry, FTMs possess both high CO_2 permeance and CO_2/N_2 selectivity[8]. This is achieved through the incorporation of certain reactive moieties (e.g., amines) that are either chemically bonded to the polymer backbone (i.e., fixed-site carrier) or dispersed in the membrane matrix (i.e., mobile carrier). These carriers control a series of fundamental physical and chemical processes, such as carrier–CO_2 reaction, guest molecule diffusion, and N_2 sorption, that determine the transport properties of the FTM.

In our previous study, we computationally evaluated these properties in amine-containing FTMs and demonstrated that the molecular diffusion and N_2 sorption were greatly affected by the water uptake values of FTMs. Our experimental measurements also revealed that by incorporating the ionic 2-(1-piperazinyl)ethylamine sarcosinate (PZEA-Sar) mobile carrier, which interacts more intensely with water molecules, the equilibrium water uptake ($WU_{eq} = m_{water}/m_{dry\ FTM} \times 100$ wt.%) of the FTM was substantially enhanced.[9] The higher water uptake promoted the diffusion of CO_2, CO_2 reaction products, and mobile carrier, resulting in a higher CO_2 permeance observed experimentally.[9] Therefore, the water uptake of the FTM is critical to its transport behavior. To this end, the determination of the equilibrium water uptake value of the FTM is necessary for the evaluation of its performance. Additional computational studies have been conducted to understand the role of water in polymeric FTMs. Fayon and Sarkisov used molecular dynamics (MD) simulations and geometric analysis to understand the diffusion behavior of water and ions in polyvinylamine (PVAm) at different water uptake values.[10] Nieto et al. adopted MD simulations to study the water contact angle on the surface of PVAm to understand the wettability of the polymer.[11] However, an efficient computational method that can predict the water sorption in FTMs has not yet been established, which inhibits accurate computational investigations of FTM performances for screening carrier candidates from the vast chemical space of amines.

One approach to predicting the equilibrium water uptake is to simulate the water sorption process explicitly from a dry FTM to equilibrium. For a given FTM configuration (i.e., geometries and orientations of the fixed-site and mobile carriers), the grand canonical Monte Carlo (GCMC) simulation can be employed to simulate its water uptake assuming the polymer matrix is rigid. Molecular dynamics (MD) simulations can subsequently be used to relax the polymer matrix and let it respond to the sorption of water molecules in order to capture the structural flexibility of the polymeric FTM. The GCMC and MD simulations are iteratively conducted until no significant changes in the water uptake can be observed. This so-called GCMC-MD approach has been exemplified by Kupgan et al. on the simulations of CO_2 plasticization in a polymer of intrinsic microporosity (PIM-1).[12] By doing so, a better agreement with the experimentally observed CO_2 loading was achieved as compared to using only GCMC simulations with a rigid PIM-1 structure.[12]

An alternative approach to the simulation of the sorption process is to evaluate the chemical potential of the adsorbate (μ_{ads}) at a given loading and determine whether it is lower or higher than that of the imaginary external gas reservoir (μ_{res}). The equilibrium loading can then be determined by finding the loading where μ_{ads} is equal to μ_{res}. The accuracy and efficiency of such an approach depend on the method employed to determine the chemical potential of the adsorbate. The Widom insertion method[13] has been widely used to probe the chemical potential of a simulation box with insertions of a ghost adsorbate molecule. However, the Widom method exhibits poor efficiency in dense systems.[14–16] Advanced sampling methods based on the original Widom method have been proposed, in which the insertion moves of the ghost particle are manipulated to favor the statistically significant regions (i.e., $\Delta U < 0$). Examples of such improvements include the accelerated Widom method[17] and grid-based Widom method[18,19]. However, these methods require extensive calibrations that are specific to the geometry of the systems studied, thus making them potentially inefficient for amorphous FTM structures. Another technique that can be used to determine the chemical potential of adsorbates is the continuous fractional component Monte Carlo (CFCMC) method.[20] During CFCMC simulations, an existing adsorbate molecule is selected as the test particle, and its interaction with the surrounding molecules is scaled with a fractional parameter, λ. The CFCMC method alters the λ parameter to sample its probability distribution, upon which the chemical potential of the adsorbate can be derived.[21] It has been shown that the CFCMC method can greatly augment the efficiency of Monte Carlo samplings for different guest molecules (e.g., Lennard-Jones particles[22] and real gases[23]), especially in dense systems (e.g., liquid water)[20,24].

In this study, we applied both the explicit water sorption simulation approach (i.e., iterative GCMC-MD simulations) and the chemical potential-based prediction approach to study the water sorption in polymeric FTMs. FTMs composing of the well-studied poly(*N*-vinylformamide-*co*-vinylamine) (PNVF-*co*-VAm, Figure 1(a)) fixed-site carrier and PZEA-Sar (Figure 1(b)) mobile carrier at different weight ratios were studied. The theoretically predicted water uptake values were compared to experimental benchmarks. At the predicted equilibrium water uptake values, the associated transport properties, including the diffusivities of gases and mobile carriers and the solubility of N_2, were also computationally investigated. We demonstrated that, by using the chemical potential-based approach with CFCMC, the water sorption in FTMs can be accurately predicted. Such an approach can be transferrable to study the water sorption of other amorphous polymers, as will be shown later, and potentially other classes of materials such as metal–organic frameworks (MOFs) with the breathing effect[25, 26].

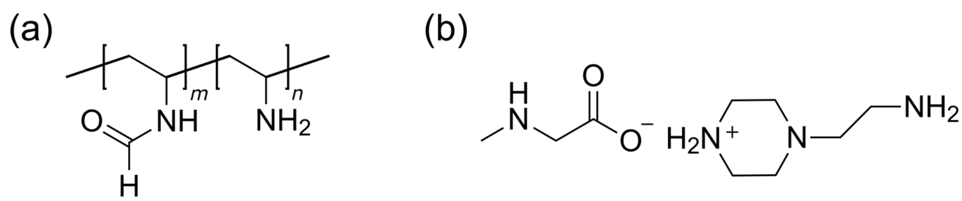

Figure 1. Structures of (a) poly(*N*-vinylformamide-*co*-vinylamine) (PNVF-*co*-VAm) and (b) 2-(1-piperazinyl)ethylamine sarcosinate (PZEA-Sar). In (a), *m* and *n* stand for the numbers of *N*-vinylformamide (NVF) and vinylamine (VAm) repeating units, respectively. The ratio of $m : n$ is 85 : 15 in this study. The protonation of VAm was not considered herein since the protonated VAm only accounted for 3% of the total repeating units.[4]

METHODS

Molecular Dynamics (MD) Simulations. MD simulations were performed using the open-source LAMMPS (large-scale atomic/molecular massively parallel simulator) package[27] to relax the FTMs in the iterative GCMC-MD simulations, generate different configurations as inputs to the chemical potential calculations, and calculate diffusivities of guest molecules and mobile carriers. Considering the amorphous nature of polymeric FTMs, three independent simulation boxes comprising calculated amounts of the PNVF-*co*-VAm fixed-site carrier with a unique repeating unit sequence, PZEA-Sar mobile carrier, and guest molecules (i.e., CO_2, N_2, and water) were constructed. The PNVF-*co*-VAm fixed-site carrier was modeled as a polymer chain of 60–240 repeating units with the first and last repeating units connected by a polymeric bond across the periodic boundary. More details can be found in Section I of the Supporting Information (SI). These simulation boxes were initially relaxed for 1 ns in the canonical (*NVT*) ensemble. A rigorous 21-step relaxation procedure[28] was then conducted to further relax the structure, followed by a 5 ns simulation in the isobaric-isothermal (*NpT)* ensemble. In the diffusivity calculations, a 30 ns MD NVT production run was performed to ensure the diffusive region was reached. The diffusivities of different components were computed based on the obtained trajectory as described in our previous study[9].

In these calculations, for atoms of the FTMs, their Lennard-Jones potential parameters were adopted from the generalized Amber force field (GAFF)[26], while the partial charges were derived using the CHelpG (charges from electrostatic potentials using a grid-based method) scheme[29] based on electrostatic potential obtained from density functional theory (DFT) calculations using Gaussian 16[30]. The force field parameters and partial charges assigned to the carrier atoms can be found in Figure S2 and Table S1–S6 of the Supporting Information of our previous work.[9] The transferable potentials for phase equilibria (TraPPE) models[31] of CO_2 and N_2 were employed, while water was described by the widely adopted extended simple point charge (SPC/E) model[32]. A time step of 1 fs was used. The temperature and pressure of MD simulations were modulated using the Nosé–Hoover thermostat and barostat with damping factors of 100 and 1000 time steps, respectively. The Lennard-Jones potential was shifted to zero at the cutoff radius of 12 Å. The long-range Coulombic interactions were computed using the particle−particle particle−mesh method[33].

Monte Carlo Calculations. The RASPA package[34] was used to perform Monte Carlo simulations, including grand canonical Monte Carlo (GCMC) and Widom insertion calculations. In all Monte Carlo simulations, the host structure (i.e., the fixed-site carrier and mobile carrier molecules) was held rigid. In GCMC calculations, Monte Carlo attempts including translation, rotation, reinsertion, and swap (insertion and deletion) moves were performed with a ratio of 1 : 1 : 2 : 4. In the Widom method, the swap moves of GCMC simulations were replaced by equal amounts of Widom insertions of the guest molecule. In all Monte Carlo simulations, 5000 equilibration steps and 50000 production steps were performed unless specified otherwise. All computational setups (e.g., force field parameters and partial charges) of the Monte Carlo simulations were kept consistent with those of the aforementioned MD simulations. The Widom method was also employed to study the N_2 solubilities in FTMs. In order to account for the amorphous nature of FTMs, 50 different configurations were obtained from the well-relaxed MD trajectories for each FTM composition. The Widom method was then applied to sample the solubility (i.e., Henry constant) of N_2 of every obtained configuration. The N_2 solubility reported for each FTM composition was averaged from the sampled configurations.

In the case of CFCMC calculations, the Brick package[21] was employed. The computational setups were identical to those mentioned above. The translation and rotation moves of the adsorbates each accounted for 25% of steps performed. The unique Lambda move, which adjusts the fractional parameter λ, accounted for another 20% of the steps. The remaining 30% were the so-called CFC Hybrid Moves, which attempted to reinsert and change the identity of the test particle. In an identical way to the GCMC simulations in RASPA, 5000 equilibration steps and 50000 production steps were conducted in all CFCMC simulations, and the host structures were held rigid. Similar to the Widom sampling, 30 configurations of the well-equilibrated systems were collected for each FTM to sample different structures of the polymer.

Chemical Potential Calculations. The chemical potential of an imaginary reservoir can be calculated based on thermodynamics using eq 1[13].

$$\mu_{res} = k_B T \ln\left(\frac{p\phi}{k_B T}\Lambda^3\right) \quad (1)$$

where k_B is the Boltzmann constant, T and p are the absolute temperature and pressure of the system, respectively, and ϕ is the fugacity coefficient of the gas reservoir derived based on the Peng-Robinson equation of state (PR-EOS)[35]. The critical properties and acentric factors used in the PR-EOS are summarized in Table S2 of the SI.[36] Λ is the De Broglie wavelength of the adsorbate molecule.

As for the Widom insertion method, the adsorbate chemical potential (μ_{ads}) is calculated based on the distribution of the test particle interaction (i.e., ΔU) following eq 2.

$$\mu_{ads} = \mu_{idg} + \mu_{excess} = k_B T \ln(\rho_{ads}\Lambda^3) - k_B T \ln\left(\langle e^{\left(-\frac{\Delta U}{k_B T}\right)}\rangle\right) \quad (2)$$

where μ_{idg} and μ_{excess} are the ideal gas and excess contributions, respectively. ρ_{ads} refers to the number density of adsorbate particles, and ΔU is the test particle interaction (i.e., the energy change of the system if the test particle were actually inserted).

In CFCMC simulations, a probability distribution of λ (i.e., $p(\lambda)$) can be developed through changing the test particle identity and adjusting λ. The μ_{ads} can then be derived as eq 3[21].

$$\mu_{ads} = \mu_{idg} + \mu_{excess} = k_B T \ln(\rho_{ads}\Lambda^3) - k_B T \ln\left(\frac{p(\lambda=1)}{p(\lambda=0)}\right) \quad (3)$$

RESULTS AND DISCUSSION

Explicit Simulation of Water Sorption. As discussed above, the water sorption of the FTM can be explicitly simulated through an intuitive approach – the iterative GCMC-MD simulations. In this study, the water sorption of the PNVF-*co*-VAm fixed-site carrier was first simulated *via* this approach. Since the GCMC simulation of water sorption is notoriously demanding[37], the iterative GCMC-MD approach can require an extremely long wall time. In order to expedite the simulation process, various starting configurations with initial water uptake values of 0–100 wt.% were built and relaxed as detailed above. Three independent simulation boxes were constructed for each starting water uptake value. A GCMC simulation at 330 K and the saturation vapor pressure of the SPC/E water model (i.e., p_{sat} = 6.0 kPa)[38], the so-called uncorrected saturation pressure as recommended by Datar et al[37], was first conducted. A 0.5 ns NpT-MD simulation at the same temperature and 1.10 atm (i.e., the operating conditions of FTMs) was then performed to relax the carrier-water configuration from GCMC. This iterative GCMC-MD cycle was repeated 100 times. Note that in order to ensure a reasonable wall time of the simulation, abbreviated GCMC simulations with 4000 equilibration steps and 10000 production steps were employed. The water uptake values averaged from all three independent seeds are summarized in Figure 2.

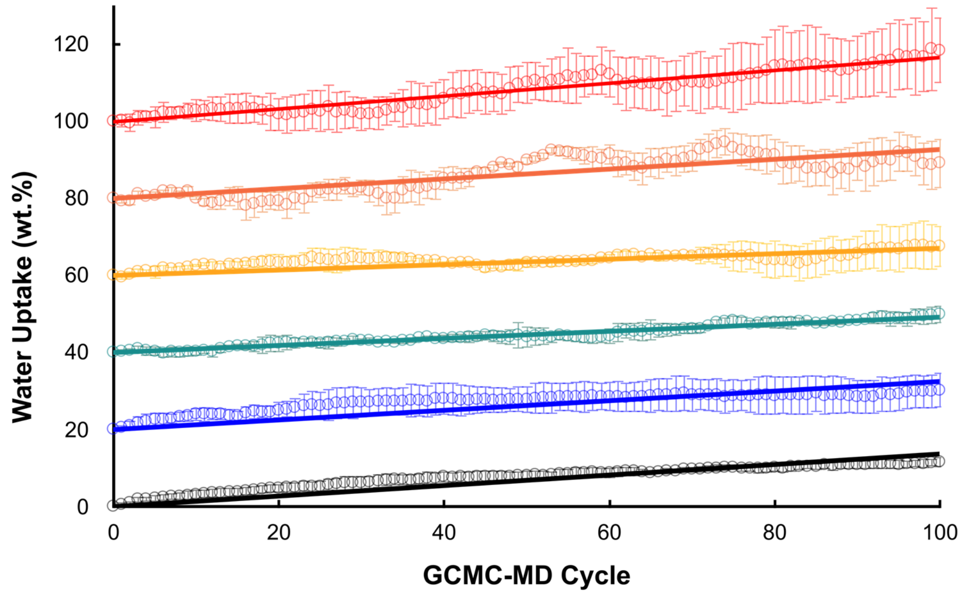

Figure 2. The water uptake values observed during the iterative grand canonical Monte Carlo (GCMC)-molecular dynamics (MD) simulations starting from initial water uptake values of 0–100 wt.%. The linear trend lines are shown to guide the eyes.

As shown, all PNVF-*co*-VAm series showed a consistent tendency of adsorbing more water into the polymer matrix. The series starting from 100 wt.% water uptake even reached a water uptake beyond 110 wt.% and showed no sign of reaching equilibrium as the water sorption was still ongoing steadily. This indicates that the equilibrium water uptake predicted by the iterative GCMC-MD approach would be substantially higher than the experimentally measured value of 75.4 wt.%[9]. Further analyses revealed that the excessive and, more importantly, seemingly non-stop water sorption behavior may be attributed to volume fluctuations of the NpT MD simulations. Consistent with Kupgan et al[12], the last frame of the MD simulation was used as the input of the next GCMC simulation. However, the sampled volume of the last frame (i.e., V) could randomly deviate from the reasonable volume of the system (i.e., average volume of equilibrated NpT MD simulation, V_{average}) owing to volume fluctuations.

Specifically, we conducted GCMC simulations for fifty configurations with different volumes sampled from a MD simulation at 100 wt.% water uptake and analyzed the water uptake change (i.e., ΔN with respect to the initial water uptake). As shown in Figure 3(a), the volume fluctuation (i.e., $V - V_{\mathrm{average}}$) of a NpT MD simulation can asymmetrically influence the ΔN predicted by the next GCMC simulation. A positive fluctuation (i.e., $V - V_{\mathrm{average}} > 0$) was found to result in more water molecules to be inserted into the polymer matrix than those deleted as a result of a negative fluctuation (i.e., $V - V_{\mathrm{average}} < 0$) of the same magnitude. Though volume fluctuations were minor (i.e., $|V - V_{\mathrm{average}}| / V_{\mathrm{average}} \leq 1.5\%$), such an asymmetric response of GCMC favoring water insertions was critical, as it led to biased water insertions accumulated through the GCMC-MD iterations and eventually resulted in the persistent water uptake growth. A potential cause of this bias is starting GCMC simulations with fully saturated configurations, where the host structures were laden with water molecules inherited from the previous MD simulations. Because of the extensive hydrogen bonds these water molecules develop with the host structure and other water molecules, they are difficult to remove, which introduces an artificial sampling bias against water deletion moves in GCMC simulations as discussed in a prior study by some of us[37].

As a follow-up analysis, we surveyed the GCMC-MD iterations starting from 100 wt.% water update, and selected twenty GCMC simulations in which the ΔN was greater than ten water molecules per simulation cell. Each of these selected GCMC simulation was reruned from the dry structure (i.e., inherited structure from MD with water molecules removed). A considerably prolonged simulation length was employed to make sure that the equilibrium water uptake value was achieved. As shown in Figure 3(b), the averaged GCMC water uptake starting from dry structures (i.e., N_{dry}) was consistently lower than those obtained starting from wet structures (i.e., N_{wet})., which confirmed that starting GCMC simulations from wet configurations indeed contributed to the bias towards water insertion.

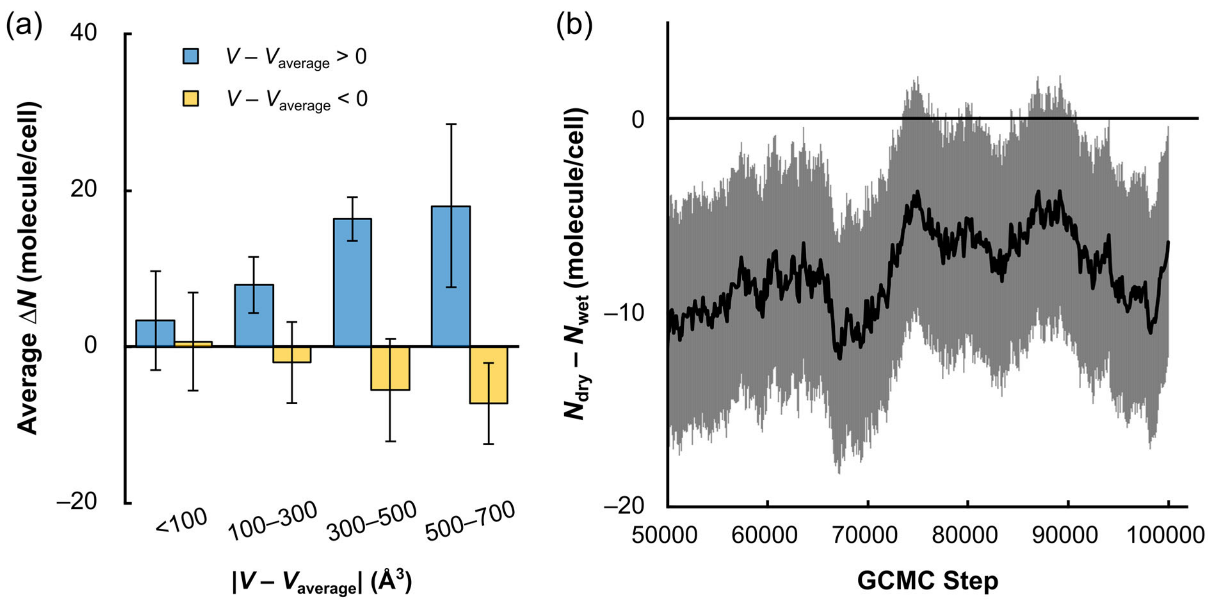

Figure 3. (a) The averaged water uptake change (ΔN with respect to the initial water uptake) computed by the GCMC simulations as a function of the absolute volume fluctuation (i.e., $|V - V_{average}|$). (b)The averaged water uptake sampled with extended GCMC simulations starting from dry configurations (N_{dry}) as compared to that of GCMC simulations starting from wet configurations (N_{wet}).

The above discussed issue can potentially be eliminated by either extending the length of GCMC simulations with wet structures or starting the GCMC simulations from dry structures.

However, both solutions would result in a prolonged wall time of each iteration and eventually make the GCMC-MD simulations prohibitively expensive. Therefore, the explicit simulation of water sorption using the iterative GCMC-MD simulations may not be suitable for describing the water sorption behavior of FTMs. It should be noted that such an excessive sorption behavior observed herein is likely to occur for adsorbates that are prone to the aforementioned sampling bias (e.g., water) in an amorphous, non-rigid host structure (e.g., polymeric FTMs), as discussed in great details above. Other sorption systems, where the adsorbate molecules do not intensely interact with each other and the host structures are of greater rigidity, may not suffer from such an issue (e.g., CO_2 in PIM-1[12]).

Chemical Potential-based Approach. An alternative approach of water sorption prediction is to derive the equilibrium water uptake value based on the chemical potential of water molecules residing in the material. The equilibrium sorption loading is reached when the chemical potential of the adsorbate is equal to that of the external reservoir. In order to quantify the chemical potential of the adsorbate, two methods, namely the Widom insertion method and the CFCMC method, were considered herein. Before applying this approach to study the complex water sorption in FTM systems, the single-gas sorption systems of CO_2 and CH_4 in the isoreticular metal–organic framework-1 (IRMOF-1) structure were first studied because of its well-defined porous structure and the available adsorption isotherms in the literature.

IRMOF-1 systems at various preset loadings (i.e., 1–220 molecules of CO_2 or CH_4) with the adsorbate molecules at thermodynamically relevant configurations were first constructed using NVT Monte Carlo simulations. The framework atoms of IRMOF-1 were described with Lennard-

Jones parameters from the DREIDING force field[39] and partial charges assigned using the multilayer connectivity-based atom contribution (m-CBAC) method[40]. The CH_4 molecule was described using a united atom model with parameters adopted from García-Pérez et al[41] while CO_2 was modeled using the TraPPE forcefield[31] as previously mentioned. The configurations obtained from the NVT simulations were then used as starting points for the Widom and CFCMC sampling of adsorbate chemical potentials. The calculated chemical potentials are presented in Figure 4(a). The chemical potentials of the reservoir at different pressure points, ranging from 0.1 to 7×10^5 kPa, were calculated using eq 1. The equilibrium loading at each pressure point of interest, where $\mu_{ads} = \mu_{res}$, can then be interpolated from the calculated chemical potential-preset loading relationship. In this study, for simplicity, linear interpolation was adopted.

For benchmark purposes, single-gas adsorption isotherms of CO_2 and CH_4 in IRMOF-1 were also calculated using the widely used GCMC simulations for the same pressure range. The GCMC isotherms obtained were found in good agreement with literature results (see Figure S2 of the SI). As shown in Figure 4(b), the adsorption isotherms derived are in excellent agreement with GCMC benchmarks. Our results confirm that through explicitly sampling the μ_{ads} at a series of preset loadings, the sorption behavior as a function of external reservoir pressure can be accurately predicted.

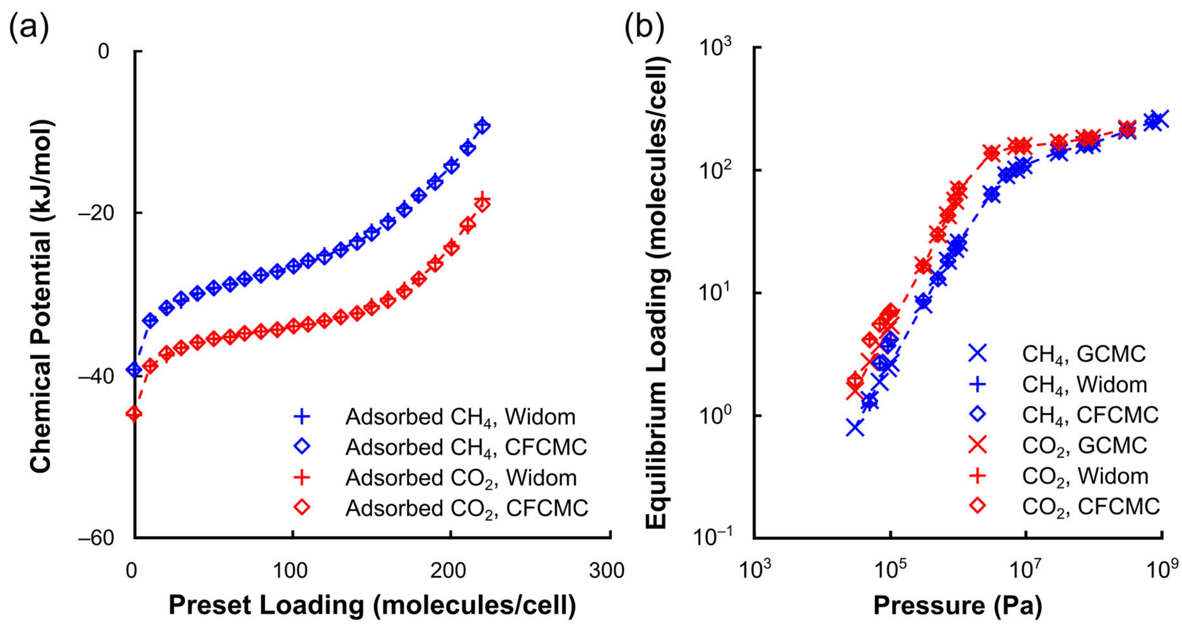

Figure 4. (a) Chemical potentials of adsorbed CO_2 and CH_4 in IRMOF-1 as a function of the preset loading sampled using the Widom or CFCMC method. (b) The adsorption isotherms simulated using GCMC and derived based on the calculated chemical potentials. The GCMC equilibrium loadings are shown for comparison.

The chemical potential-based approach was then used to predict the water sorption in the FTM consisting of only PNVF-*co*-VAm. A procedure similar to that detailed above was followed. Three independent PNVF-*co*-VAm polymer chains (i.e., seeds) were firstly constructed with preset water uptake values of 1–150 wt.% and relaxed using MD simulations. For each seed, 30 configurations, which were obtained from the last 1.5 ns of MD trajectory, were adopted. These configurations were used as starting points for sampling the adsorbed water chemical potentials using the Widom or CFCMC method. The average chemical potentials of water in PNVF-*co*-VAm at different preset water uptake values are summarized in Figure 5(a). The chemical potentials of water vapor reservoirs at different levels of relative humidity (RH) were calculated using eq 1. The equilibrium water uptake values were then interpolated similarly for the determination of adsorption isotherms in IRMOF-1 detailed above and are summarized in Figure 5(b). The choice of water model was discussed in Section IV of the SI. the In order to validate the accuracy of our theoretical predictions, the equilibrium water uptake values of PNVF-*co*-VAm were experimentally measured at RH levels of 11%, 75%, and 100% at 330 K following the procedure detailed in our previous publication[9]. Saturated LiCl and NaCl solutions were employed in this study to maintain the relative humidity at 11% and 75% RH, respectively[42], while deionized water was used to maintain the RH level at 100%.

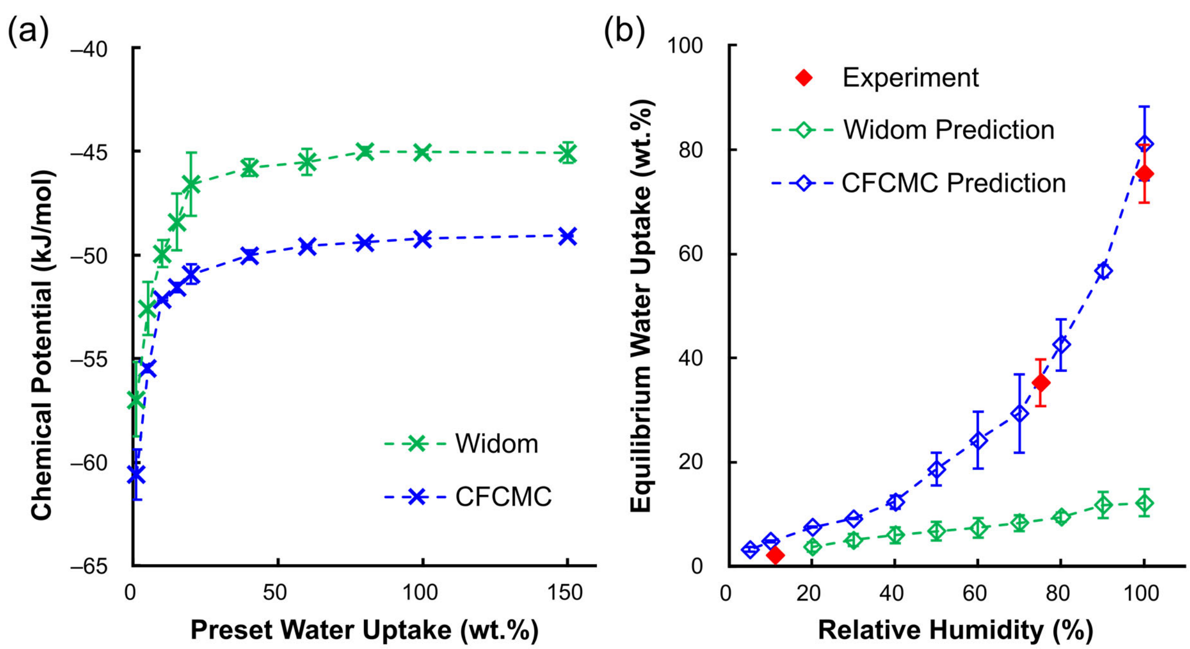

Figure 5. (a) Chemical potentials of adsorbed water in PNVF-*co*-VAm sampled using the Widom and CFCMC methods at different preset water uptake values and (b) the predicted equilibrium water uptake values at different levels of relative humidity (RH) as compared to experimental measurements.

As shown, the CFCMC method successfully reproduced the experimental water sorption values of PNVF-*co*-VAm. It can also be observed that in both computational and experimental measurements, the water uptake value of PNVF-*co*-VAm increases with the RH. As discussed in our previous publication, the increasing water uptake value significantly benefitted the CO_2 diffusion.[9] Therefore, at higher levels of RH, the FTM is expected to demonstrate higher CO_2 permeance, which is in line with experimental observations by Deng et al.[43] Moreover, we note that the chemical potential-based water sorption prediction method with CFCMC can be transferable to study the water sorption behavior of other polymers. As an example, the equilibrium water uptake values of polyvinylalcohol (PVA) at 298.15 K at different levels of RH were also computed, and the results were found in line with literature experimental values[44]. The readers are referred to Section V of the SI for more information.

In contrast to the good performance of the CFCMC method, the Widom method substantially underestimated the equilibrium water uptake values (Figure 5(b)) since it seemingly overestimated the adsorbed water chemical potential (Figure 5(a)). This can be attributed to its inefficiency when studying dense systems as discussed earlier. At higher preset water uptake values, the system is increasingly saturated with water molecules. Therefore, the test particle insertion moves of the Widom method becomes less efficient, as the chance of finding a non-repulsive or even favorable interaction site (i.e., $\Delta U \leq 0$) becomes diminishingly low. In order to capture those rare cases where the test particle interacts favorably with its surrounding, orders of magnitude more random trials need to be conducted.[17] On the other hand, the CFCMC method employs the fractional parameter λ and exhibits a higher efficiency. In addition, the CFCMC method uses existing adsorbates as test particles instead of relying on randomly positioned probes. Therefore, it was able to sample water chemical potentials in FTMs with a greater efficiency.

In order to further develop the comparison between Widom and CFCMC, the chemical potentials of liquid water at temperatures ranging from 300 to 475 K were sampled using both methods. The benchmark chemical potentials of the corresponding saturated water vapor reservoirs (i.e., at corresponding p_{sat}[38]) were also calculated using eq 1. As shown in Figure 6, the CFCMC method demonstrated a near-perfect agreement with the reference values. This clearly evidences the efficiency and accuracy of the CFCMC method when applied to dense systems. By contrast, the Widom method consistently yielded higher chemical potentials; even extending the the simulations by ten times (i.e., Widom (10×)) only led to a marginal improvement.

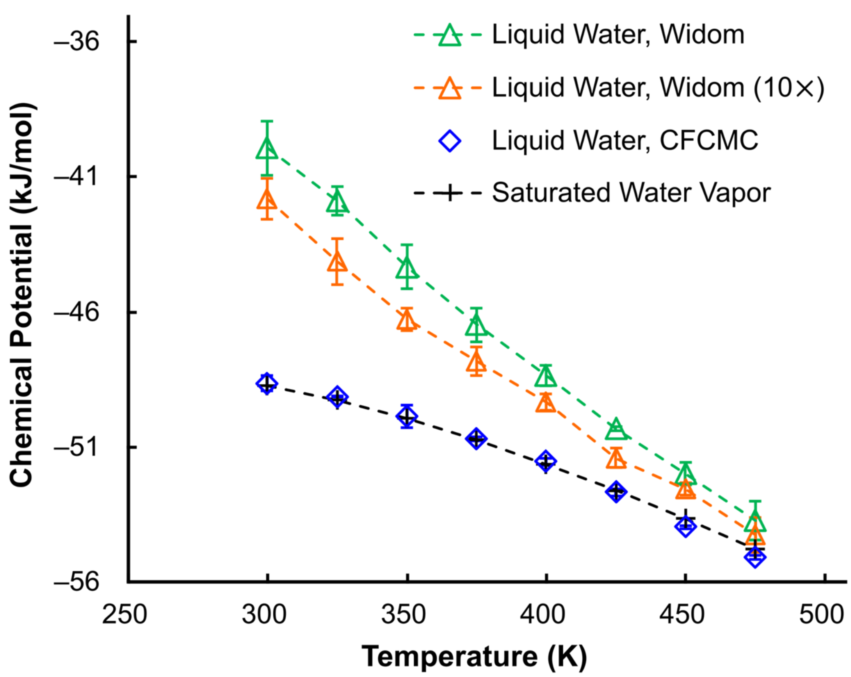

Figure 6. The chemical potentials of liquid water at different temperatures sampled using the Widom and CFCMC methods. Results from the extended Widom (i.e., Widom (10×)) simulations

were also shown. The chemical potentials of the corresponding saturated water vapor were calculated using eq 1 and are shown as benchmarks.

PZEA-Sar Content and FTM Performance. With the capability of predicting water sorption in FTMs, the effect of membrane composition on the FTM transport properties can be further discussed. Mobile carriers have been shown to significantly influence the membrane performance of FTMs.[3, 4] Previously, we demonstrated experimentally that the addition of the PZEA-Sar mobile carrier significantly augmented the equilibrium water uptake of FTMs.[9] Such enhanced water sorption behavior was expected since the ionic structure of PZEA-Sar exhibited stronger interactions with surrounding water molecules and thus made the FTM structure more hydrophilic. In order to systematically evaluate the role of the PZEA-Sar mobile carrier in FTMs and quantitatively understand their enhancement effect on water sorption, the equilibrium water uptake values of FTMs containing 10–85 wt.% PZEA-Sar with balancing PNVF-*co*-VAm were computationally determined using the aforementioned chemical potential-based approach. Specifically, the adsorbed water chemical potentials at preset water uptake values of 50–400 wt.% were calculated using CFCMC and are summarized in Figure 7(a). Three independent systems (i.e., seeds) were considered for each membrane composition.

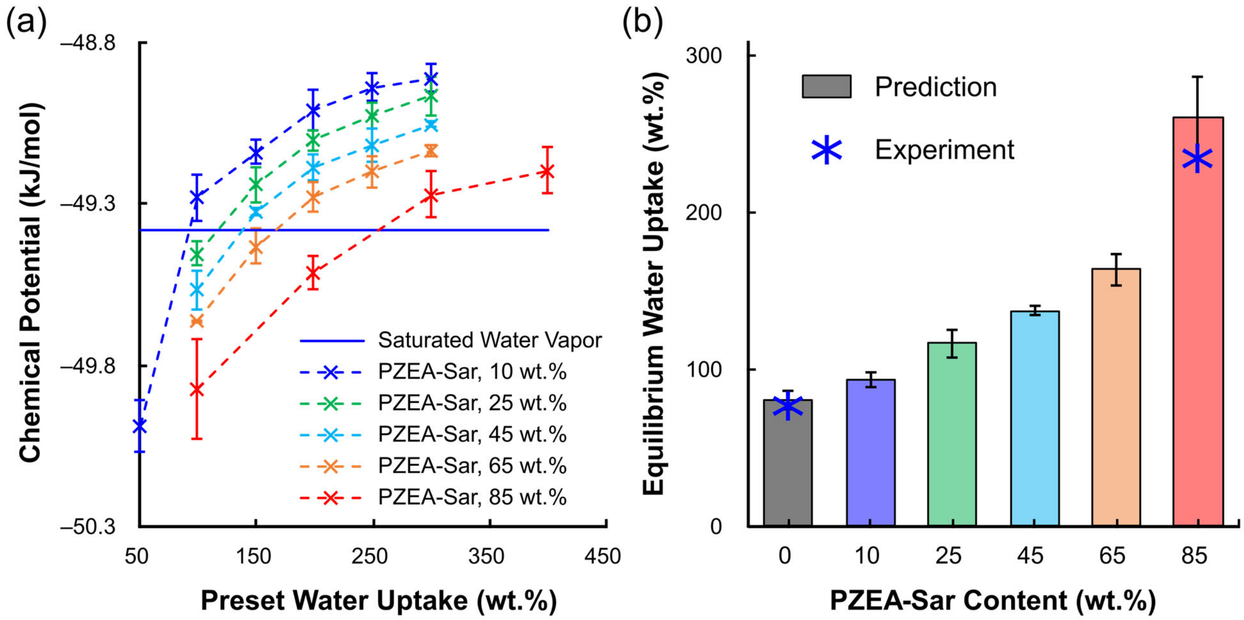

Figure 7. (a) Chemical potentials of the adsorbed water in FTMs with different PZEA-Sar contents calculated using CFCMC. The chemical potential of the saturated water vapor at 330 K is shown as the blue line. (b) The predicted equilibrium water uptake as a function of the PZEA-Sar content of the FTM. Experimental water uptake values of FTMs containing 0 wt.% and 85 wt.% PZEA-Sar are also shown in (b) for comparison.[9]

The equilibrium water uptake values calculated with error bars are summarized in Figure 7(b). As seen, the calculations showed that incorporating 85 wt.% PZEA-Sar to the PNVF-*co*-VAm fixed-site carrier indeed significantly increased the equilibrium water uptake value from 81.2 wt.% to 259.4 wt.%, which is in line with the experimental observation. Further analysis also confirmed that PZEA-Sar intensified water-carrier interactions as demonstrated in Figure S7, where adding 85 wt.% PZEA-Sar enhanced the water-carrier interaction by –12.3 kcal/mol at the water uptake of 100 wt.% as compared to the FTM with pure PNVF-*co*-VAm. This intensified water-carrier interaction consequently reduced the excess chemical potential of adsorbed water and eventually resulted in a larger equilibrium water uptake value at a higher PZEA-Sar content.

With the equilibrium water uptake values of FTMs established, we further discuss how the mobile carrier content affects the CO_2 and N_2 permeation and eventually the FTM performance. In order to comment on the CO_2 permeation behavior, we have focused on the diffusivities of CO_2 and the PZEA-Sar mobile carrier. These diffusivities were computationally evaluated in FTMs with 0–85 wt.% PZEA-Sar at their respective computed equilibrium water uptake values, and the results are summarized in Figure 8(a) with the mean sqaured displacement (MSD) shown in Figure S5. As seen, benefitting from a greater equilibrium water uptake value, a higher PZEA-Sar content substantially promoted the diffusion of CO_2 and the mobile carrier as their diffusivities approaching the values in bulk water (i.e., 2.90×10^{-5} and 7.57×10^{-6} cm^2/s, respectively, based on MD simulations), thus facilitating the permeation of both unreacted and reacted CO_2. This could be attributed to the wider diffusion channels at high water uptake values as demonstrated in Figure S6. The enhanced permeation of CO_2 naturally leads to a higher CO_2 permeability and permeance, which is in line with the growing CO_2 permeance observed experimentally in FTMs with 45–85 wt.% PZEA-Sar[4].

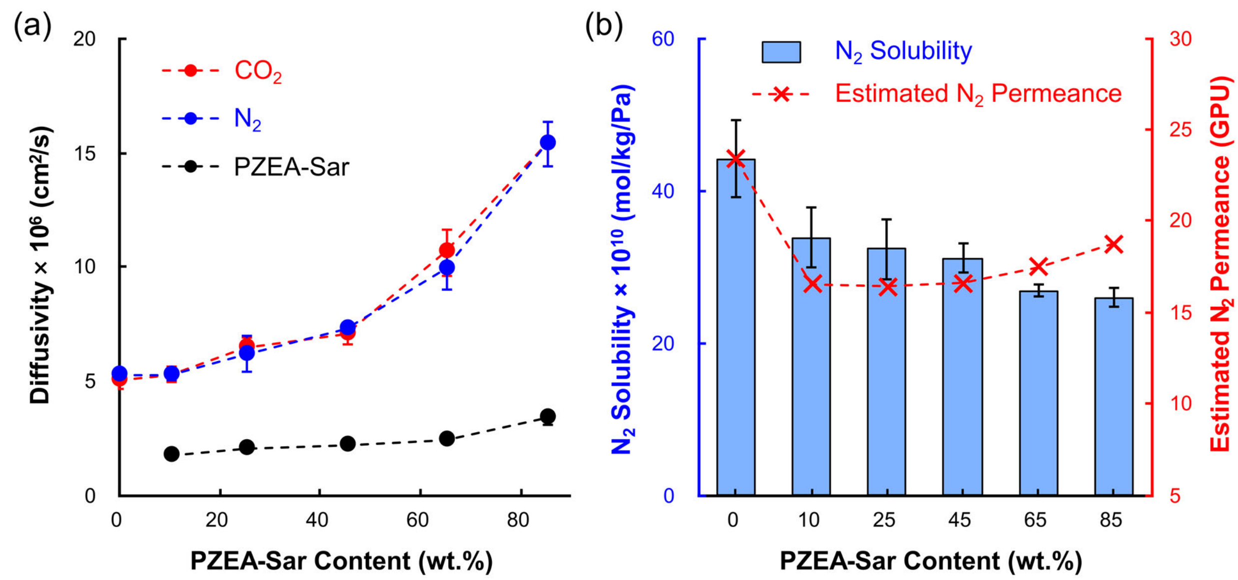

Figure 8. (a) The diffusivities of CO_2, N_2, and the PZEA-Sar mobile carrier and (b) N_2 solubility and estimated N_2 permeance in FTMs with 0–85 wt.% PZEA-Sar mobile carrier at corresponding equilibrium water uptake values. In (b), a dry active layer thickness of 170 nm was used in the N_2 permeance estimations of all PZEA-Sar contents.

Also shown in Figure 8(a) are the calculated N_2 diffusivities at different PZEA-Sar contents. The N_2 diffusivity also increased with PZEA-Sar content and approached the value in bulk water (i.e., 2.74×10^{-5} cm^2/s). However, the higher N_2 diffusivity was countered by the decreasing N_2 solubility, which is depicted in Figure 8(b). This can be attributed to the suppressing effect of water molecules on N_2 sorption by saturating the N_2 adsorption sites.[9] We note that because of the reactive nature of CO_2 in FTMs, its solubility could not be calculated using the Widom method as employed for N_2. Instead, the CO_2 loading capacity of different carriers can be probed by their reaction chemistry, which was not expected to be heavily influenced by the water uptake.

Since the N_2 permeation follows the solution-diffusion mechanism, the N_2 permeability (P_{N_2}) can be calculated using eq 4.

$$P_{N_2} = D_{N_2} \times S_{N_2} \quad (4)$$

where D_{N_2} and S_{N_2} are the computationally determined diffusivity and solubility of N_2 in the FTM. With a dry thickness (l_{dry}) of 170 nm, which is the typical selective layer thickness[1,4,7], the thickness of the fully swollen selective layer (l_{wet}) can be calculated using eq 5.

$$l_{wet} = (l_{dry} \cdot \rho_{dry} \cdot \frac{WU_{eq.}+100\ wt.\%}{100\ wt.\%})/\rho_{wet} \quad (5)$$

where ρ_{dry} and ρ_{wet} are the densities of the dry and fully hydrated selective layers and WU_{eq} is the equilibrium water uptake (i.e., $m_{water}/m_{dry\ FTM} \times 100$ wt.%). The ρ_{dry} and ρ_{wet} values were sampled from the last 2 ns of the well-equilibrated NpT-MD simulations. Finally, the N_2 permeances (P_{N_2}/l_{wet}) of FTMs with 0–85 wt.% PZEA-Sar at their respective equilibrium water uptake values were estimated and are shown in Figure 8(b). As illustrated, the addition of 10 wt.% PZEA-Sar reduced the N_2 permeance considerably owing to the suppressed N_2 solubility and thicker selective layer. As the PZEA-Sar further increased, the decrease in N_2 solubility and the increase in selective layer thickness became less significant, while the increase in N_2 diffusivity became more prominent. Therefore, the N_2 permeance gradually increased. However, even at a high PZEA-Sar content of 85 wt.%, the N_2 permeance still did not exceed the value of the FTM with only PNVF-*co*-VAm. This observation is also in agreement with the lower N_2 permeance experimentally observed in the FTM with 85 wt.% PZEA-Sar as compared to the FTM with only PNVF-*co*-VAm[4].

Based on these theoretical findings, the role of PZEA-Sar in FTMs can be illustrated. With its stronger affinity to water, the addition of PZEA increased the hydrophilicity of the membrane.

This enhanced the water uptake of the FTM at the operating conditions. The higher equilibrium water uptake values, in turn, promoted the diffusion of CO_2 and mobile carrier, thus facilitating CO_2 permeation. The N_2 diffusivity increased at the same time. But since the N_2 sorption was stifled and the active layer became thicker, the incorporation of PZEA-Sar suppressed the N_2 permeation of FTMs as compared to the FTM containing only the PNVF-*co*-VAm fixed-site carrier in general.

CONCLUSIONS

In this study, we systematically evaluated two approaches to predicting the equilibrium water uptake values of FTMs. The explicit simulation of water sorption using the iterative GCMC-MD simulations led to a persistently increasing water uptake even beyond the experimentally measured equilibrium water uptake value of PNVF-*co*-VAm. The chemical potential-based prediction approach instead demonstrated its viability and reasonably predicted the water sorption behavior in FTMs with PNVF-*co*-VAm at different levels of relative humidity, as well as the equilibrium water uptake values of FTMs with 10–85 wt.% PZEA-Sar contents with balancing PNVF-*co*-VAm. In line with experimental observations, the higher PZEA-Sar content increased the water uptake value of the FTM. As a result, the addition of PZEA-Sar promoted the diffusion of unreacted and reacted CO_2 and suppressed N_2 sorption. This is also in line with the higher CO_2 permeance and CO_2/N_2 selectivity experimentally observed in the FTM with 85 wt.% PZEA-Sar as compared to the FTM with only PNVF-*co*-VAm. To the best of our knowledge, this is a first-of-a-kind study where the water sorption in FTMs was computationally predicted and validated against experimental measurements. The chemical potential-based prediction approach used herein can be transferable to study other polymeric systems. The ability to predict the equilibrium water uptake values of FTMs with different compositions also allows us to computationally screen the vast chemical space of amines to discover better-performing carrier structures.

ASSOCIATED CONTENT

Supporting Information

The Supporting Information is available free of charge on the ACS Publications website at DOI: XXXXXX.

Carrier compositions of facilitated transport membranes (FTMs), critical properties and acentric factors of CO_2, CH_4, and water, adsorption isotherms of CH_4 and CO_2 in IRMOF-1, water sorption predictions using other water models, water uptake predictions of polyvinylalcohol (PVA), mean squared displacement (MSD) data of diffusivity calculations, snapshots of simulated FTMs with 0–85 wt.% PZEA-Sar at equilibrium water uptake values, and water-carrier interactions at different PZEA-Sar contents.

AUTHOR INFORMATION

Corresponding Authors

*E-mail: han.779@osu.edu (Y.H.).

*E-mail: lclin@ntu.edu.tw (L.-C.L.).

*E-mail: ho.192@osu.edu (W.S.W.H.).

Author Contributions

The manuscript was written through contributions from all authors.

Notes

The authors declare no competing financial interest.

ACKNOWLEDGMENTS

X. D. thanks Dr. Remco Hens for insightful advice on implementing the Brick package. L.-C. L. also appreciates the support from the Yushan Young Program from the Ministry of Education in Taiwan (NTU-110VV009). The authors gratefully acknowledge the Department of Energy – National Energy Technology Laboratory (DE-FE0031731) for the financial support of this work. This work was partly supported by the Department of Energy under Award Numbers DE-FE0031731 with substantial involvement of the National Energy Technology Laboratory, Pittsburgh, PA, USA. The authors also gratefully acknowledge the computational resources from the Ohio Supercomputer Center (OSC).[45]

REFERENCES

(1) Chen, K. K.; Salim, W.; Han, Y.; Wu, D.; Ho, W. S. W. Fabrication and Scale-up of Multi-Leaf Spiral-Wound Membrane Modules for CO_2 Capture from Flue Gas. *J. Membr. Sci.* **2020**, *595*, 117504.

(2) Vakharia, V.; Salim, W.; Wu, D.; Han, Y.; Chen, Y.; Zhao, L.; Ho, W. S. W. Scale-up of Amine-Containing Thin-Film Composite Membranes for CO_2 Capture from Flue Gas. *J. Membr. Sci.* **2018**, *555*, 379–387.

(3) Chen, Y.; Zhao, L.; Wang, B.; Dutta, P.; Ho, W. S. W. Amine-Containing Polymer/Zeolite Y Composite Membranes for CO_2/N_2 Separation. *J. Membr. Sci.* **2016**, *497*, 21–28.

(4) Han, Y.; Wu, D.; Ho, W. S. W. Nanotube-Reinforced Facilitated Transport Membrane for CO_2/N_2 Separation with Vacuum Operation. *J. Membr. Sci.* **2018**, *567*, 261–271.

(5) Han, Y.; Wu, D.; Ho, W. S. W. Simultaneous Effects of Temperature and Vacuum and Feed Pressures on Facilitated Transport Membrane for CO_2/N_2 Separation. *J. Membr. Sci.* **2019**, *573*, 476–484.

(6) Tong, Z.; Ho, W. S. W. Facilitated Transport Membranes for CO_2 Separation and Capture. *Sep. Sci. Technol.* **2017**, *52*, 156–167.

(7) Han, Y.; Salim, W.; Chen, K. K.; Wu, D.; Ho, W. S. W. Field Trial of Spiral-Wound Facilitated Transport Membrane Module for CO_2 Capture from Flue Gas. *J. Membr. Sci.* **2019**, *575*, 242–251.

(8) Han, Y.; Ho, W. S. W. Polymeric Membranes for CO_2 Separation and Capture. *J. Membr. Sci.* **2021**, *628*, 119244.

(9) Deng, X.; Zou, C.; Han, Y.; Lin, L.-C.; Ho, W. S. W. Computational Evaluation of Carriers in Facilitated Transport Membranes for Postcombustion Carbon Capture. *J. Phys. Chem. C* **2020**, *124*, 25322–25330.

(10) Fayon, P.; Sarkisov, L. Structure and Dynamics of Water in Molecular Models of Hydrated Polyvinylamine Membranes. *Phys. Chem. Chem. Phys.* **2019**, *21*, 26453–26465.

(11) Romero Nieto, D.; Lindbråthen, A.; Hägg, M. B. Effect of Water Interactions on Polyvinylamine at Different PHs for Membrane Gas Separation. *ACS Omega* **2017**, *2*, 8388–8400.

(12) Kupgan, G.; Demidov, A. G.; Colina, C. M. Plasticization Behavior in Polymers of Intrinsic Microporosity (PIM-1): A Simulation Study from Combined Monte Carlo and Molecular Dynamics. *J. Membr. Sci.* **2018**, *565*, 95–103.

(13) Frenkel, D.; Smit, B. *Understanding Molecular Simulation: From Algorithms to Applications*, 2nd ed; Academic Press: San Diego, 2002.

(14) Tripathi, S.; Chapman, W. G. An Algorithm for Calculating the Chemical Potential in Associating and Reacting Fluids. *Mol. Phys.* **2003**, *101*, 1199–1209.

(15) Neimark, A. V.; Vishnyakov, A. A Simulation Method for the Calculation of Chemical Potentials in Small, Inhomogeneous, and Dense Systems. *J. Chem. Phys.* **2005**, *122*, 234108.

(16) Hörstermann, H.; Hentschke, R.; Amkreutz, M.; Hoffmann, M.; Wirts-Rütters, M. Predicting Water Sorption and Volume Swelling in Dense Polymer Systems via Computer Simulation. *J. Phys. Chem. B* **2010**, *114*, 17013–17024.

(17) Dömötör, G.; Hentschke, R. Atomistically Modeling the Chemical Potential of Small Molecules in Dense Systems. *J. Phys. Chem. B* **2004**, *108*, 2413–2417.

(18) Alema, C.; Mun, S.; Zanuy, D.; Leo, S. Molecular Simulation of Gas Solubilities in Crystalline Poly (a-Alkyl-b-l-Aspartate) S. *Polymer (Guildf).* **2000**, *41*, 4169–4177.

(19) Zanuy, D.; Alemán, C.; López-Carrasquero, F.; Báez, M. E.; García-Alvarez, M.; Laso, M.; Muñoz-Guerra, S. On the Phase B of Comb-like Poly(a-Alkyl-β-L-Aspartate)s: A Simulation of the Solubility of Small Penetrants. *Macromol. Chem. Phys.* **2001**, *202*, 564–573.

(20) Shi, W.; Maginn, E. J. Continuous Fractional Component Monte Carlo: An Adaptive Biasing Method for Open System Atomistic Simulations. *J. Chem. Theory Comput.* **2007**, *3*, 1451–1463.

(21) Hens, R.; Rahbari, A.; Caro-Ortiz, S.; Dawass, N.; Erdös, M.; Poursaeidesfahani, A.; Salehi, H. S.; Celebi, A. T.; Ramdin, M.; Moultos, O. A.; et al. Brick-CFCMC: Open Source Software for Monte Carlo Simulations of Phase and Reaction Equilibria Using the Continuous Fractional Component Method. *J. Chem. Inf. Model.* **2020**, *60*, 2678–2682.

(22) Poursaeidesfahani, A.; Hens, R.; Rahbari, A.; Ramdin, M.; Dubbeldam, D.; Vlugt, T. J. H. Efficient Application of Continuous Fractional Component Monte Carlo in the Reaction Ensemble. *J. Chem. Theory Comput.* **2017**, *13*, 4452–4466.

(23) Rahbari, A.; Poursaeidesfahani, A.; Torres-Knoop, A.; Dubbeldam, D.; Vlugt, T. J. H. Chemical Potentials of Water, Methanol, Carbon Dioxide and Hydrogen Sulphide at Low Temperatures Using Continuous Fractional Component Gibbs Ensemble Monte Carlo. *Mol.*

Simul. **2018**, *44*, 405–414.

(24) Poursaeidesfahani, A.; Torres-Knoop, A.; Dubbeldam, D.; Vlugt, T. J. H. Direct Free Energy Calculation in the Continuous Fractional Component Gibbs Ensemble. *J. Chem. Theory Comput.* **2016**, *12*, 1481–1490.

(25) Neimark, A. V.; Coudert, F. X.; Boutin, A.; Fuchs, A. H. Stress-Based Model for the Breathing of Metal-Organic Frameworks. *J. Phys. Chem. Lett.* **2010**, *1*, 445–449.

(26) Coudert, F. X.; Boutin, A.; Fuchs, A. H.; Neimark, A. V. Adsorption Deformation and Structural Transitions in Metal-Organic Frameworks: From the Unit Cell to the Crystal. *J. Phys. Chem. Lett.* **2013**, *4*, 3198–3205.

(27) Plimpton, S. Fast Parallel Algorithms for Short-Range Molecular Dynamics. *J. Comput. Phys.* **1995**, *117*, 1–19.

(28) Abbott, L. J.; Hart, K. E.; Colina, C. M. Polymatic: A Generalized Simulated Polymerization Algorithm for Amorphous Polymers. *Theor. Chem. Acc.* **2013**, *132*, 1–19.

(29) Breneman, C. M.; Wiberg, K. B. Determining Atom-centered Monopoles from Molecular Electrostatic Potentials. The Need for High Sampling Density in Formamide Conformational Analysis. *J. Comput. Chem.* **1990**, *11*, 361–373.

(30) Frisch, M. J.; Trucks, G. W.; Schlegel, H. B.; Scuseria, G. E.; Robb, M. A.; Cheeseman, J. R.; Scalmani, G.; Barone, V.; Petersson, G. A.; Nakatsuji, H. et al. *Gaussian 16*, Revision A.03. Gaussian, Inc.: Wallingford, CT, 2016.

(31) Potoff, J. J.; Siepmann, J. I. Vapor-Liquid Equilibria of Mixtures Containing Alkanes, Carbon Dioxide, and Nitrogen. *AIChE J.* **2001**, *47*, 1676–1682.

(32) Berendsen, H. J. C.; Grigera, J. R.; Straatsma, T. P. The Missing Term in Effective Pair Potentials. *J. Phys. Chem.* **1987**, *91*, 6269–6271.

(33) Darden, T.; York, D.; Pedersen, L. Particle Mesh Ewald: An $N \cdot \log(N)$ Method for Ewald Sums in Large Systems. *J. Chem. Phys.* **1993**, *98*, 10089–10092.

(34) Dubbeldam, D.; Calero, S.; Ellis, D. E.; Snurr, R. Q. RASPA: Molecular Simulation Software for Adsorption and Diffusion in Flexible Nanoporous Materials. *Mol. Simul.* **2016**, *42*, 81–101.

(35) Peng, D.; Robinson, D. B. A New Two-Constant Equation of State A New Two-Constant Equation of State. *Ind. Eng. Chem. Fundam.* **1976**, *15*, 59–64.

(36) Poling, B. E.; Prausnitz, J. M.; O'Connell, J. P. *The Properties of Gases and Liquids*, 5th ed.; McGraw-Hill: New York, 2001.

(37) Datar, A.; Witman, M.; Lin, L.-C. Improving Computational Assessment of Porous Materials for Water Adsorption Applications via Flat Histogram Methods. *J. Phys. Chem. C* **2021**, *125*, 4253–4266.

(38) SAT-TMMC: Liquid-Vapor coexistence properties - SPC/E Water (LRC) https://www.nist.gov/mml/csd/informatics/sat-tmmc-liquid-vapor-coexistence-properties-spce-water-lrc (accessed May 1, 2021).

(39) Mayo, S. L.; Olafson, B. D.; Goddard, W. A. DREIDING: A Generic Force Field for Molecular Simulations. *J. Phys. Chem.* **1990**, *94*, 8897–8909.

(40) Zou, C.; Penley, D. R.; Cho, E. H.; Lin, L.-C. Efficient and Accurate Charge Assignments via a Multilayer Connectivity-Based Atom Contribution (m-CBAC) Approach. *J. Phys.*

Chem. C **2020**, *124*, 11428–11437.

(41) García-Pérez, E.; Parra, J. B.; Ania, C. O.; García-Sánchez, A.; Van Baten, J. M.; Krishna, R.; Dubbeldam, D.; Calero, S. A Computational Study of CO_2, N_2, and CH_4 Adsorption in Zeolites. *Adsorption* **2007**, *13*, 469–476.

(42) Greenspan, L. Humidity Fixed Points of Binary Saturated Aqueous Solutions. *J. Res. Natl. Bur. Stand.* **1977**, *81*, 89–96.

(43) Deng, L.; Hägg, M. B. Swelling Behavior and Gas Permeation Performance of PVAm/PVA Blend FSC Membrane. *J. Membr. Sci.* **2010**, *363*, 295–301.

(44) Popescu, M. C. Structure and Sorption Properties of CNC Reinforced PVA Films. *Int. J. Biol. Macromol.* **2017**, *101*, 783–790.

(45) Ohio Supercomputer Center. http://osc.edu/ark:/19495/ f5s1ph73 (accessed June 1, 2020).

TOC Graphic

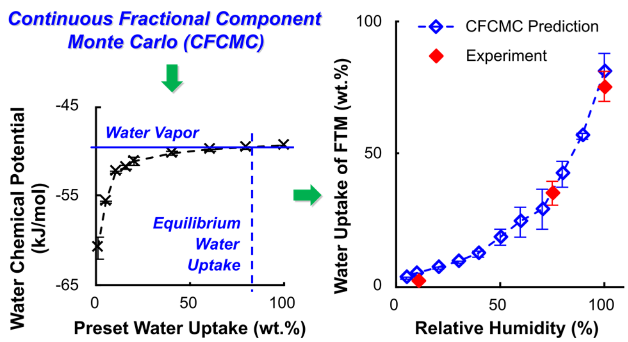

Continuous Fractional Component Monte Carlo (CFCMC)
Water Vapor
Equilibrium Water Uptake
Water Chemical Potential (kJ/mol)
Preset Water Uptake (wt.%)
CFCMC Prediction
Experiment
Water Uptake of FTM (wt.%)
Relative Humidity (%)